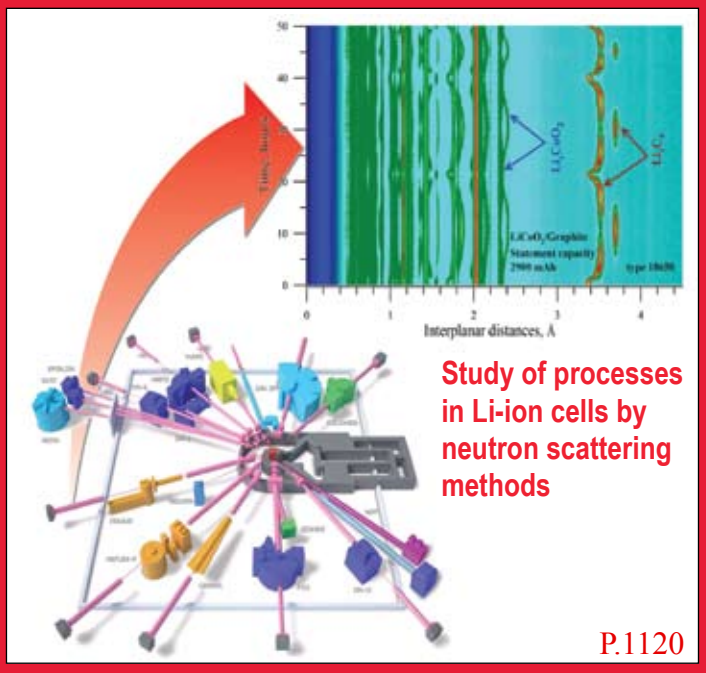
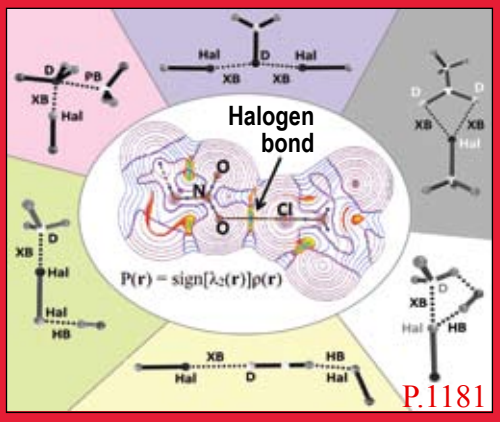
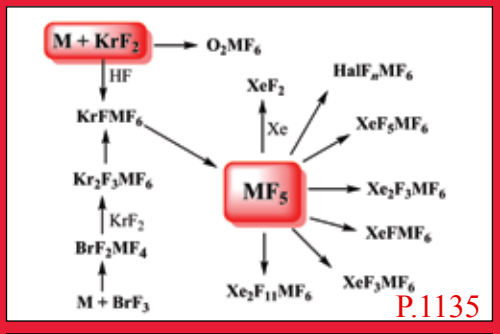
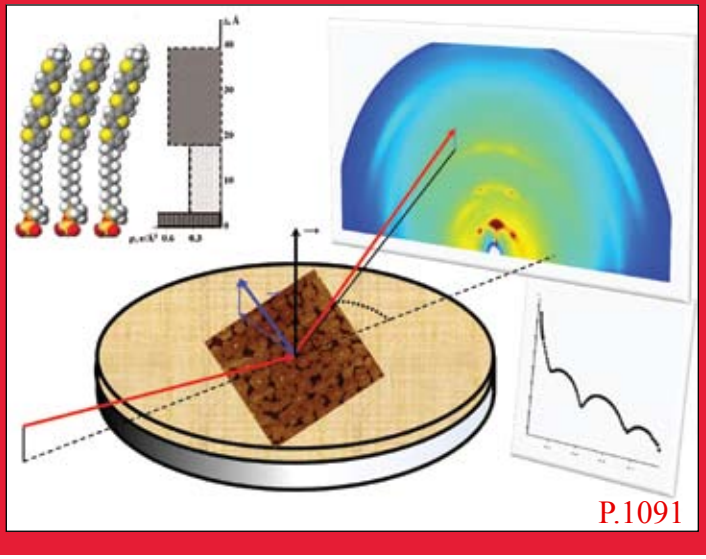
ISSN 0036-021X

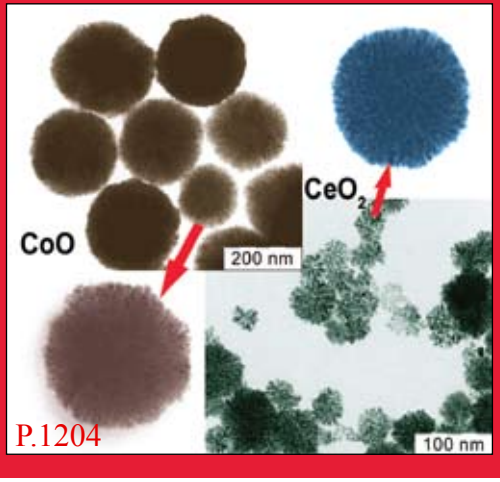
Russian Chemical Reviews











Reviews on current topics in chemistry

International Year of Crystallography

Volume 83 2014 Number 12

 © 2014 Russian Academy of Sciences and Turpion Ltd

DOI 10.1070/RCR4473

Neutron scattering for analysis of processes in lithium-ion batteries

A M Balagurov,[a] I A Bobrikov,[a] N Yu Samoylova,[a, b] O A Drozhzhin,[c] E V Antipov [c]

[a] *Frank Laboratory of Neutron Physics, Joint Institute for Nuclear Research ul. Joliot-Curie 6, 141980 Dubna, Russian Federation*
[b] *Skobeltsyn Institute of Nuclear Physics, Lomonosov Moscow State University Leninskie Gory 1, bld. 2, 119234 Moscow, Russian Federation*
[c] *Department of Chemistry, Lomonosov Moscow State University Leninskie Gory 1, bld. 3, 119991 Moscow, Russian Federation*

The review is concerned with analysis and generalization of information on application of neutron scattering for elucidation of the structure of materials for rechargeable energy sources (mainly lithium-ion batteries) and on structural rearrangements in these materials occurring in the course of electrochemical processes. Applications of the main methods including neutron diffraction, small-angle neutron scattering, inelastic neutron scattering, neutron reflectometry and neutron introscopy are considered. Information on advanced neutron sources is presented and a number of typical experiments are outlined. The results of some studies of lithium-containing materials for lithium-ion batteries, carried out at IBR-2 pulsed reactor, are discussed.
The bibliography includes 50 references.

Contents

I. Introduction 1120
II. Interaction of neutrons with matter: specific features 1122
III. Neutron structural studies of power cells: the potential and main avenues of current research 1122
IV. Neutron scattering experiments at the IBR-2 reactor: a survey 1128
V. Conclusion 1133

A M Balagurov Doctor of Physical and Mathematical Sciences, Professor, Chief researcher of Frank Laboratory of Neutron Physics, JINR.
Telephone (7-496) 216 58 03, e-mail: bala@nf.jinr.ru
I A Bobrikov Candidate of Physical and Mathematical Sciences, Researcher of the same Laboratory.
Telephone (7-496) 216 65 80, e-mail: bobrikov@nf.jinr.ru
N Yu Samoylova Candidate of Physical and Mathematical Sciences, Researcher of the same Laboratory and Department for Nuclear Research of the SINP MSU.
Telephone (7-496) 216 22 53, e-mail: samoylova@jinr.ru
O A Drozhzhin Candidate of Chemical Sciences, Researcher of the Chemistry Department, MSU.
Telephone (7-496) 216 65 80, e-mail: drozhzhin@hotmail.com
E V Antipov Corresponding Member of the Russian Academy of Sciences, Doctor of Chemical Sciences, Professor, Head of Division of Electrochemistry of the same Department.
Telephone (7-495) 939 33 75, e-mail: antipov@icr.chem.msu.ru
Current research interests: electrochemical power sources, inorganic materials, lithium-ion cells, solid oxide fuel elements, superconductors, crystal structure.

Received 25 June 2014
Uspekhi Khimii **83** (12) 1120 – 1134 (2014); translated by A M Raevskiy

I. Introduction

At present, interdisciplinary research of novel electrode materials for lithium-ion batteries is rapidly progressing. This is due to the need for solving problems related to gradual depletion of natural sources of energy, deterioration of environmental conditions and energy saving. The main advantages of lithium-ion batteries compared to other types of power cells include a much higher specific stored energy and a larger number of reversible charge – discharge cycles. This is to a great extent determined by the properties of the electrode materials, first of all, cathode materials. The most practically important properties of a cathode material are as follows:

— high specific capacity;

— high potential of the redox process occurring during the extraction (incorporation) of lithium and simultaneous oxidation (reduction) of the transition metal;

— high electronic and lithium ion conductivities; and

— small volume changes accompanying the charge – discharge processes.

These key properties of the cathode material are mainly governed by the crystal structure. Therefore, crystal chem-

ical studies play the most important role in the design of novel cathode materials for lithium-ion batteries and in the optimization of their electrochemical properties.

The $LiCoO_2$ compound was chosen as cathode material for lithium-ion batteries based on analysis of its crystal structure (α-$NaFeO_2$ structural type derived from the NaCl structure). Layer-by-layer ordered arrangement of lithium and cobalt cations predetermines the possibility of fast 2D transport of lithium for reversible intercalation processes occurring during cell charge–discharge.[1] In a decade, this discovery became a scientific basis to progress in production of lithium-ion power cells for portable electronic devices. Rapid increase in production of lithium-ion batteries and extension of their application fields (up to utilization in electric vehicles, robotics, airplanes and steady-state large-scale energy storage units for accumulation of energy from renewable sources and load levelling in electricity mains) dictate the need for improvement of their operating characteristics, as well as corresponding safety requirements, environmental profile and price. Intensive research made it possible to offer new classes of cathode materials with the spinel ($LiMn_2O_4$), olivine ($LiFePO_4$), NASICON [$Li_3Fe_2(PO_4)_3$], wurtzite (Li_2FeSiO_4) structures, as well as transition metal sulfates, fluorophosphates and fluorosulfates that possess the ability to reversibly intercalate lithium.

In 1997, Goodenough and co-workers[2] reported $LiFePO_4$ as safe, cheap and environmentally benign material for rechargeable lithium batteries. This result is of great value because it leads to considerable extension of possible fields of the search for novel materials among inorganic compounds with polyanionic groups. Such materials are more stable than complex oxides under heat treatment and multiple cycling. Their crystal structures are well documented (see, *e.g.*, reviews 3 and 4).

Naturally, crystallographic methods of investigation are widely used to elucidate specific features of the structure of cathode materials for lithium-ion batteries including their transient states formed in the course of the charge–discharge cycles. The most widely used methods include X-ray (synchrotron) diffraction and electron microscopy. Neutron diffraction is used much more rarely, but advanced neutron sources and a number of unique features of the interaction of neutrons with matter gradually make this method valuable for studying the structure of cathode materials and processes occurring in the course of cell charge–discharge.

The atomic and magnetic structures of materials used for batteries, power cells and fuel cells and structural changes under the action of external factors are successfully studied using the diffraction of thermal neutrons with a characteristic energy of about 0.02 eV and a characteristic wavelength of nearly 1.8 Å. Recently, neutron diffraction has also been used to study the transient phenomena accompanying electrochemical processes in materials for power sources. Moreover, this method of investigation was employed to analyze the behaviour of the cathode and anode materials not only in the model electrochemical cells adapted to meet the conditions for neutron diffraction experiments, but also in the commercially available cells. The advantages of neutron diffraction appeared to be so important that the last decade was marked by the beginning of experiments with different types of electrochemical cells in most advanced neutron research centres.

Neutron diffraction is the main method for obtaining information on the structure of crystalline materials on the atomic level (*i.e.*, on the length scale of a few fractions of a nanometre). In addition, power cells are intensively studied by small-angle neutron scattering, neutron reflectometry and neutron introscopy. These methods provide information on the behaviour of matter (not necessarily in the crystalline state) on the length scales next to the atomic level. Namely, small-angle neutron scattering and neutron reflectometry enable analysis of structural features with characteristic sizes from a few nanometres to tens (in some cases, hundreds) of nanometres. Neutron introscopy usually works at a level of a few tens of micrometres. Inelastic and quasi-elastic neutron scattering data allow one to extract information on the dynamics of atomic vibrations and, therefore, on the character of interatomic interactions and diffusion processes in the medium.

A number of reviews devoted to specific features of the interaction of thermal neutrons with matter and to experimental procedures for *in situ* neutron diffraction studies at steady-state neutron sources are available (see, *e.g.*, Refs 5 and 6). These features are of importance from the standpoint of research on electrode materials. Recently, studies on lithium-ion batteries carried out at advanced pulsed neutron sources using the time-of-flight technique, which offers some new options in the *in situ* experiments, have been reported.[7, 8]

This review concerns applications of neutron diffraction and some other types of neutron scattering to examination of the structure of materials for lithium-ion batteries and transient phenomena in them. We will outline the potential of advanced neutron sources and describe a number of typical experiments. Also, the results of recently started diffraction studies of lithium-containing materials and lithium-ion batteries at the IBR-2 pulsed reactor at the Joint Institute for Nuclear Research (Dubna, Moscow Region, Russia) will be discussed.

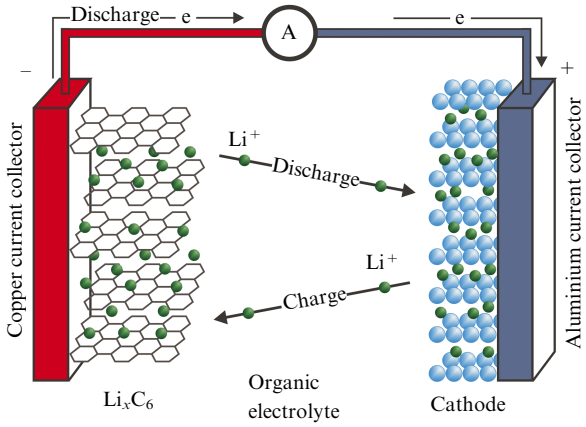


Figure 1. A schematic view of a lithium-ion battery.
Shown are the discharge and charge processes.
During discharge, lithium ions pass from anode (initially, graphite) through a separator (organic electrolyte) to cathode ($LiCoO_2$, $LiFePO_4$ and other materials).
During charge, lithium ions pass from cathode to anode.
Current collectors: metallic plates usually made of copper or aluminium.

A schematic of a typical lithium-ion battery is presented in Fig. 1. Shown are the charge and discharge processes, main materials that contribute to the diffraction pattern in the *in situ* experiments, namely, the anode (Li_xC_6), cathode ($Li_{1-x}CoO_2$), current collectors (usually, they are made of Cu and Al) and an organic electrolyte separating the anode and cathode. During the charge of the cell, the anode (in this case, a specially prepared graphite) is gradually intercalated with lithium and goes to the LiC_6 state. Besides $LiCoO_2$, cathodes are made of, *e.g.*, mixed oxides containing lithium, nickel, manganese and cobalt ($Li_xNi_yMn_zCo_{1-y-z}O_2$), lithium iron phosphate ($LiFePO_4$), *etc*. The characteristic time of diffusion of Li^+ cations and corresponding structural changes in the cell materials is of the order of a few tens of minutes at an optimum charge rate. This gives the estimate of the time needed to measure the neutron diffraction patterns with acceptable statistics in the real-time experiments.

II. Interaction of neutrons with matter: specific features

Studies on the structure of materials for power sources and processes occurring in them should be carried out taking into account the following specific features of the interaction of thermal neutrons with matter, which fundamentally distinguish thermal neutrons from X-rays (synchrotron radiation):

— high sensitivity to light elements;

— ability to distinguish between elements with close atomic numbers;

— ability to distinguish between isotopes;

— independence of the coherent scattering length on the momentum transfer;

— large magnetic scattering cross-section; and

— large penetration depth.

It is these features that make neutron experiments a source of information that usually cannot be obtained by other methods.

Light elements (hydrogen, lithium, carbon, oxygen, fluorine) are of paramount importance for the operation of electrical current sources and knowledge of their distribution in the structure of materials is necessary for understanding the redox processes. X-Rays either are blind to these elements or give insufficient accuracy in the determination of corresponding atomic positions in the structure. A classical field of application of neutron diffraction includes elucidation of the atomic structure of hydrides and oxides. The intensity of a neutron diffraction peak is determined by the coherent scattering length (b) which, in contrast to the coherent scattering length of X-rays, can be either positive or negative. For the light elements, one has

Element	H	Li	C	O	F
b /fm	−3.74	−1.90	6.65	5.80	5.65

(From this point on, the scattering lengths are given in *fermi*, 1 fm = 10^{-13} cm). The b values of cations as constituents of electrode materials are of the same order of magnitude as those of the light elements

Element	Mn	Co	Ni
b /fm	−3.73	2.49	10.30

Many electrode materials for power sources contain different types of cations. An example is provided by the oxide $Li_{1.2}Mn_{0.4}Ni_{0.3}Co_{0.1}O_2$, a candidate for being a cathode material for lithium-ion batteries.[9] 3d-Metals scatter X-rays almost identically; therefore, their distribution over crystallographic positions and possible ordering can be best determined only using neutron diffraction.

In some complicated cases, atomic positions in the structure are refined using isotope contrast, especially if the isotope scattering lengths differ not only in magnitude, but also in sign. This first of all concerns hydrogen and lithium isotopes. For instance, replacement of hydrogen ($b_H = -3.74$) by deuterium ($b_D = 6.67$) provides a way to reliable refinement of corresponding atomic positions in the structure and to the determination of their accessibility to exchange. This also holds for the lithium isotopes characterized by $b = 2.00$ (^{6}Li) and $b = -2.22$ (^{7}Li). In addition to neutron diffraction, isotope substitution is widely used in small-angle neutron scattering studies to attain a more pronounced contrast between particular regions of multiphase systems.

Owing to specific features of the nuclear interaction of neutrons with atoms the coherent scattering length is independent of the momentum transfer. Correspondingly, a decrease in the intensities of neutron diffraction peaks with increasing the momentum transfer is due to thermal motion of atoms only, whereas in the case of X-ray scattering one deals with a noticeable effect of the atomic form factor. This feature allows one to significantly extend the observed range of interplanar spacings and to more reliably determine the parameters of thermal motion.

The interaction of thermal neutrons with atomic magnetic moments is comparable in strength with the nuclear interaction of neutrons. This makes it possible to obtain information on the magnetic structure of matter, *viz*., positions, magnitudes and directions of magnetic moments in the neutron diffraction experiments. Undoubtedly, this information is of importance when using materials based on the 3d elements (Ni, Mn, Co, Fe) in which temperature variations can induce magnetic phase transitions affecting their macroscopic properties.

The absorption cross-sections of thermal neutrons are large only for a few isotopes of rare-earth elements and for ^{6}Li (power cells utilize a natural mixture of lithium isotopes which is characterized by low neutron absorption), ^{10}B and ^{113}Cd. The absorption cross-sections of most other elements and isotopes (in particular, all 3d metals) are of the order of a few barns (1 b = 10^{-24} cm^2). Correspondingly, the linear absorption coefficients of thermal neutrons are thousands of times lower than those of X-rays. High penetrability of thermal neutrons makes it possible to use a relatively simple design of *in situ* experiments with model electrochemical cells and actual power cells representing 3D objects.

III. Neutron structural studies of power cells: the potential and main avenues of current research

At present, there are nearly 20 neutron research sources and many of them are used to study electrochemical power cells. Successful research requires that the following requirements be met:

— the neutron source should have a relatively high mean power, *viz*., >10 MW for a steady-state reactor and >200 kW for a pulsed source;

— there should be a high-resolution neutron diffractometer (HRD) with $\Delta d/d \approx 2 \times 10^{-3}$ (d is the interplanar spacing) for high-precision determination of the atomic structure;

— there should be a high-intensity neutron diffractometer (HID) for *in situ* experiments (so-called '*operando*' conditions), such that measurements of the total neutron diffraction spectrum from a conventional 1-cm^3 polycrystalline sample (*e.g.*, Al_2O_3 ceramics) take a few minutes;

— the HID should provide simultaneous measurements of a large interval of interplanar spacings (at least from 0.7 to 10 Å); and

— there should be devices to specify and maintain external conditions (temperature, composition of the gaseous medium, humidity, *etc.*) for samples and electrochemical cells for *in situ* experiments.

Only a few neutron research centres meet these requirements to the full extent. This first of all concerns the HFR (ILL, France), SINQ (PSI, Switzerland), FRM-II (TUM, Germany), NIST (USA) and ANSTO (Australia) steady-state neutron sources, the ISIS (United Kingdom), SNS (USA) and J-SNS (Japan) pulsed neutron sources. The one and only appropriate neutron research facility in the Russian Federation is the IBR-2 pulsed reactor.

Experiments using steady-state sources (these are conventional nuclear reactors except SINQ) are carried out using neutron spectrometers with monochromatic neutron beams. In this case, the neutron diffraction patterns are functions of the scattering angle (Fig. 2 *a*). Diffraction experiments with monochromatic beams are carried out using the same procedure irrespective of the source type (neutron, X-ray or synchrotron radiation source).

An example of *in situ* experiments is provided by a study [10] of a commercially available lithium-ion battery

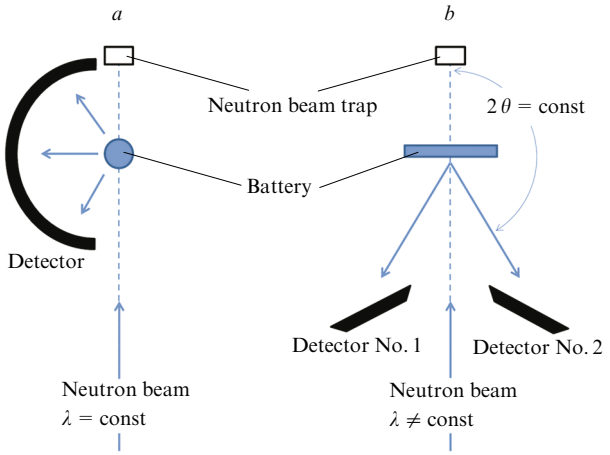


Figure 2. Typical geometries for experiments with monochromatic (*a*) and 'white' (*b*) neutron beams.
At λ = const, scattered neutrons are detected by a large position-sensitive detector with scanning the scattering angle. In the case of 'white' neutron beam, several individual detectors positioned at fixed scattering angles are used. The neutron diffraction pattern is scanned by the neutron wavelength. Cylindrical shape of the cell is optimum for scanning the scattering angle.

$45 \times 45 \times 5$ mm in size having a $LiCoO_2$ cathode. Experiments were carried out with a Wombat neutron diffractometer (λ = 2.41 Å). A position-sensitive detector covered a scattering angle of 120°, which made it possible to collect the neutron diffraction spectra in the interplanar spacing range of $1.35 \leqslant d_{hkl} \leqslant 6.28$ Å. The experiment involved a total of 1.5 charge–discharge cycles (discharge, charge and final discharge of the cell); the neutron diffraction patterns were measured continuously every 5 min over a period of 59 h.

It was established that the cathode material represents a mixture of the layered and cubic (spinel type) polymorphs of $LiCoO_2$. Both polymorphs participate in lithium insertion/extraction processes passing *via* a number of structural states. For the fully charged cell, only 64% of the graphite anode material transformed to the final state, LiC_6; the remaining phases had lower lithium content.

Experiments at pulsed neutron sources are usually carried out in a wide wavelength range using the time-of-flight (TOF) technique. Correspondingly, the neutron diffraction patterns are functions of the neutron wavelength (Fig. 2 *b*). Here, one can accumulate the neutron diffraction and other spectra at fixed positions of the sample and detectors, which makes it possible to choose an optimum orientation of the cell (or battery) relative to the directions of the incident and scattered neutron beams. However, it should be noted that the experiments using diffractometers with monochromatic neutron beams give more accurate structural data because a smaller number of corrections are required in this case in converting the integrated intensities into structure factors.

Structural changes in two compounds [based on $LiMO_2$ (M = Ni, Mn, Co) with different content of lithium and different cations M] in the course of cycling in an electrochemical cell were compared.[8] *In situ* experiments were carried out at the VULCAN beamline, the diffraction spectra were measured in the interplanar spacing range of $0.5 \leqslant d_{hkl} \leqslant 2.5$ Å; the neutron source, SNS, was operational at 800 kW average power, the neutron diffraction data were measured every 60 min. No complete structural analysis of the data collected was performed, only the changes in the unit cell parameters of anode (graphite) and cathode were analyzed quantitatively. It was established that the lithium-exess material is characterized by irreversible structural changes during the first charge–discharge cycle; this was attributed to oxygen loss from the structure (*cf.* reversible structural changes in the classical compound $LiNi_{1/3}Mn_{1/3}Co_{1/3}O_2$).

Steady-state and pulsed neutron sources should not be treated as alternatives. Different experimental designs lead to somewhat different results in the studies of the same objects using diffractometers with close main parameters (intensity, resolution). The main reasons are as follows:

— different ranges of interplanar spacings;

— different signal-to-background ratio in different spectral regions; and

— different corrections applied in converting the integrated intensities into structure factors.

In complicated situations, a joint analysis of experimental data collected at the steady-state and pulsed neutron sources usually makes it possible to draw more substantiated conclusions.

III.1. Neutron diffraction studies of power sources: main avenues of research

There is considerable literature on applications of neutron diffraction to studies of power cells and one can list the main avenues of scientific research:

— structural analysis of novel electrode materials;

— studies on structural transitions in electrode materials upon changes in external conditions;

— *in situ* studies of structural processes in electrodes in the course of redox reactions in model conditions;

— *in situ* studies of structural processes in electrode materials in commercially available devices; and

— investigation of structural degradation of electrode materials.

The type of a neutron diffractometer is specified by the problem to be solved and by the complexity of the structure of the material. Usually, studies begin with experiments at rather high-intensity, moderate-resolution diffractometers. Subsequent high-precision structural analysis is performed at high-resolution diffractometers. *In situ* experiments are carried out with specific high-intensity diffractometers in real time.

Investigation of the microstructure of electrode materials and the state of their surface in the cells may become an important application of neutron scattering, because both factors to a great extent determine their operating properties (see, *e.g.*, Ref. 11). However, research in this field is in the early stage of development owing to complexity of the problem.

In the text below we will illustrate the aforesaid by examples of experimental studies of power cells.

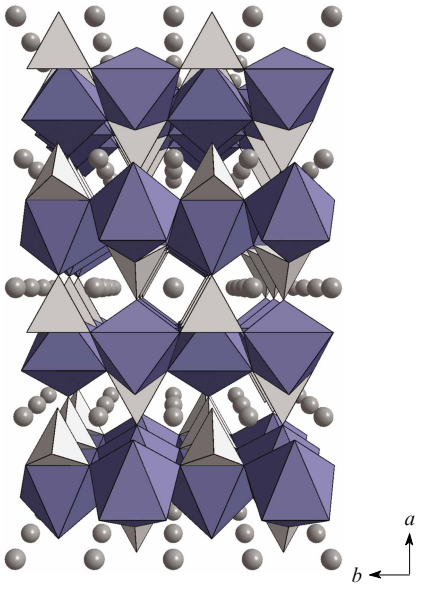


Figure 3. General view of the structure of $LiFePO_4$ (space group *Pnma*).
Shown are the FeO_6 octahedra, PO_4 tetrahedra and lithium ions in voids between them.

III.2. Examples of neutron diffraction studies

III.2.a. Structural analysis of lithium-containing materials

Carrying out neutron structural analysis of Li-containing materials requires that specific features of the interaction of neutrons with lithium atoms be taken into account. A natural mixture of lithium isotopes (92.5% ^{7}Li and 7.5% ^{6}Li) is characterized by a small negative coherent neutron scattering length $b_{coh} = -1.90$ fm. This enables reliable determination of positions of lithium ions in the unit cell among other atoms characterized by positive scattering lengths. Lithium isotopes have strongly different absorption cross-sections (0.045 b for ^{7}Li and 940 b for ^{6}Li), so the use of the ^{7}Li isotope may significantly improve the quality of experimental data in complicated situations. However, oxides usually contain at most 20% of lithium and the use of the natural mixture of lithium isotopes is admissible.

The paper [12] is a good example of a neutron diffraction refinement of the atomic and magnetic structures of $LiFePO_4$ (widely used cathode material) and its delithiated form $FePO_4$ is available.[12] That study was aimed at comparing the magnetic structures of these materials that have the same lattice type but differ in Li content and iron valence (Fe^{2+} and Fe^{3+}, respectively). Structurally, $LiFePO_4$ is built of slightly distorted FeO_6 octahedra and PO_4 tetrahedra with Li^+ ions occupying voids between these polyhedra (Fig. 3). The neutron diffraction data were collected at the D20 high-intensity diffractometer (ILL, Grenoble, France) using a powdered sample ($\sim$1 g) of the material under study; thorough measurements were performed in the temperature range from 2 to 300 K. It was confirmed that $LiFePO_4$ and $FePO_4$ have the same type of the atomic structure, *viz.*, the *Pnma* space group; the lattice constants are as follows:

Parameter /Å	*a*	*b*	*c*
$LiFePO_4$	10.338	6.011	4.695
$FePO_4$	9.760	5.752	4.756

The accuracy of determination of the interatomic spacings between cations and the oxygen atom varied from 0.002 to 0.004 Å. The onset of long-range antiferromagnetic ordering on cooling was detected at 52 K in $LiFePO_4$ and at 125 K in $FePO_4$. The refined value of the magnetic moment of Fe^{2+} in $LiFePO_4$ at 2 K was 4.19(5) μ_B. This is slightly higher than the maximum possible spin moment value (4 μ_B) and can seemingly be explained by some orbital contribution to the total magnetic moment. The magnetic moment of Fe^{3+} in $FePO_4$ at 2 K is 4.15(3) μ_B, which is slightly lower than the nominal spin moment of this cation (5 μ_B). For both compounds, configurations of the magnetic moments of iron ions correspond to the A-type antiferromagnetic structure with small G-type contribution for $FePO_4$; this agrees with the results of symmetry analysis.

Structural analysis [9, 13] of lithium-containing compositions $LiMn_{1/3}Ni_{1/3}Co_{1/3}O_2$ and $Li_{1.2}Mn_{0.4}Ni_{0.3}Co_{0.1}O_2$ was aimed to determine factors influencing the occupancy of crystallographic sites by cations. Based on the results of analysis of the X-ray and neutron diffraction data and resonant X-ray scattering data, a system of constrains on the occupancy of particular sites by cations was introduced, and correlation between parameters became much less pronounced.

Structure refinement of the first composition assuming the *R*-3*m* group showed that Mn, Ni and Co atoms are randomly distributed over sites in the basal plane of the

hexagonal structure, which also contains 2% of Li ions that replace Ni cations. This was explained by the fact that the charge state of nickel in this structure is 2+ and the ionic radius of Ni^{2+} (0.83 Å) is close to that of Li^{+} (0.9 Å). The change in the cationic composition in the second, lithium-rich, compound led to a fundamental structural rearrangement, in particular, its symmetry reduced from rhombohedral to monoclinic. Most Ni^{3+} ions are in the low-spin state and the ionic radius of Ni^{3+} (0.7 Å) is close to those of Mn^{4+} (0.67 Å) and low-spin Co^{3+} (0.685 Å). The distribution of manganese and nickel cations over possible structural sites is noticeably different from random distribution; contrary to this, the distribution of cobalt cations is close to random one. It should be noted that the stoichiometry $Li_{1.165(36)}Mn_{0.402(13)}Ni_{0.323(16)}Co_{0.109(32)}O_2$ determined from neutron diffraction data is in good agreement with the initially assumed one.

The sites of lithium ions in the structure can be fixed with the necessary accuracy (~0.01 Å) while the occupancy of structural sites by cations can be determined with an error of a few per cent.[9,12] It is this accuracy that is optimum for analysis of structural features that influence the diffusion of lithium in the course of charge–discharge processes.

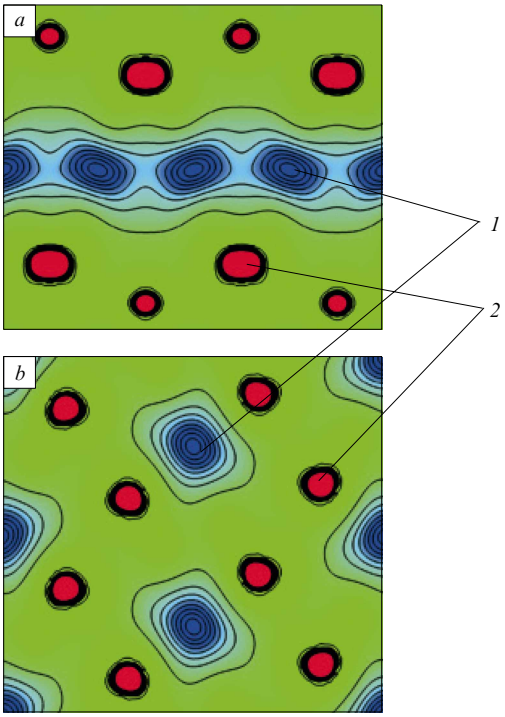


Figure 4. Nuclear coherent scattering length density map (b_{coh}) for $Li_{0.6}FePO_4$ (T = 620 K), calculated by the MEM using neutron diffraction data.[15]
(*a*) The unit cell cross-section plane is perpendicular to the *c* axis (z = 0.5), the horizontal axis is directed along the [010] direction; at high temperature, lithium delocalizes along slightly curved 1D chains along the [010] direction; (*b*) the unit cell cross-section plane is perpendicular to the *b* axis (y = 0.5), the horizontal axis is directed along the [100] direction.
(*1*) Negative density (lithium nuclei), (*2*) positive density (Fe, P and O nuclei).

III.2.b. Determination of possible diffusion paths of lithium ions from neutron diffraction data

Visualization of diffusion pathways of lithium ions is a topical task in structural analysis of compounds with lithium-ion conductivity. A series of studies carried out in a research group headed by M Yashima (see his review [14]) illustrates how one can monitor a gradual transition from thermal vibrations to continuous diffusion of lithium ions using neutron diffraction data collected in variable-temperature experiments and an analysis of the scattering nuclear density distribution by the maximum entropy method (MEM).

A detailed description of this approach was exemplified by Li_xFePO_4.[15] Experiments were carried out with a ^{7}Li-enriched powdered sample (99.9% enrichment) in order to reduce absorption and incoherent background and to increase contrast. Data were collected using two different neutron diffractometers, one of them at a pulsed neutron source (TOF technique was used) and the other at a steady-state reactor. These diffractometers are complementary with respect to the range of momentum transfer and resolution; these data arrays were subsequently processed jointly.

A preliminary X-ray diffraction analysis revealed the existence of a single-phase $Li_{0.6}FePO_4$ with themodynamically stabilized defects in a narrow temperature range from 600 to 630 K. The Rietveld method was used for structure refinement and then was followed by calculations of the coherent scattering length density maps for different cross-sections of the unit cell. The maps for two cross-sections of the unit cell (see Fig. 4) clearly demonstrate delocalization of lithium ions along the [010] direction (*Pnma* space group). It is natural to assume that it is this direction along which lithium ions diffuse in the $LiFePO_4$ cathode.

Similar calculations [14] for other ionic conductors showed that the diffusion pathways are solely determined by the structural features of particular compounds. For instance, migration of lithium ions in $La_{0.62}Li_{0.16}TiO_3$ occurs along the [110] directions (*Cmmm* space group) at z = 0.5, thus being of 2D character.

III.2.c. Studies on structural rearrangements in electrode materials: model experiments

The arrangement of chemical power sources is quite complicated being characterized by presence of various materials and complex topology of their location. Correspondingly, the neutron diffraction patterns from electrode materials are often too complicated and of low quality. In many cases, attempts to extract detailed information on structural rearrangement in the electrode materials during charge–discharge processes fail. The problem can be solved using model electrochemical cells with realistic designs that are somewhat simpler, first of all, geometrically.

Electrochemical cells adapted to operation with particular compounds using neutron diffractometers have been documented (see, *e.g.*, Refs 16–28). Initially, the cells for *in situ* neutron diffraction studies of electrode materials had a cylindrical geometry and contained ~5 g of sample. Such a cell [16] (Fig. 5 *a*) was constructed for a neutron diffraction study of lithium extraction from $Li_xMn_2O_4$ at a steady-state reactor (Studsvik, Sweden). The composition of the final state, $Li_{0.85}Mn_2O_4$, was determined from the neutron diffraction patterns. The content of lithium was in agreement with the results of determination from the total charge

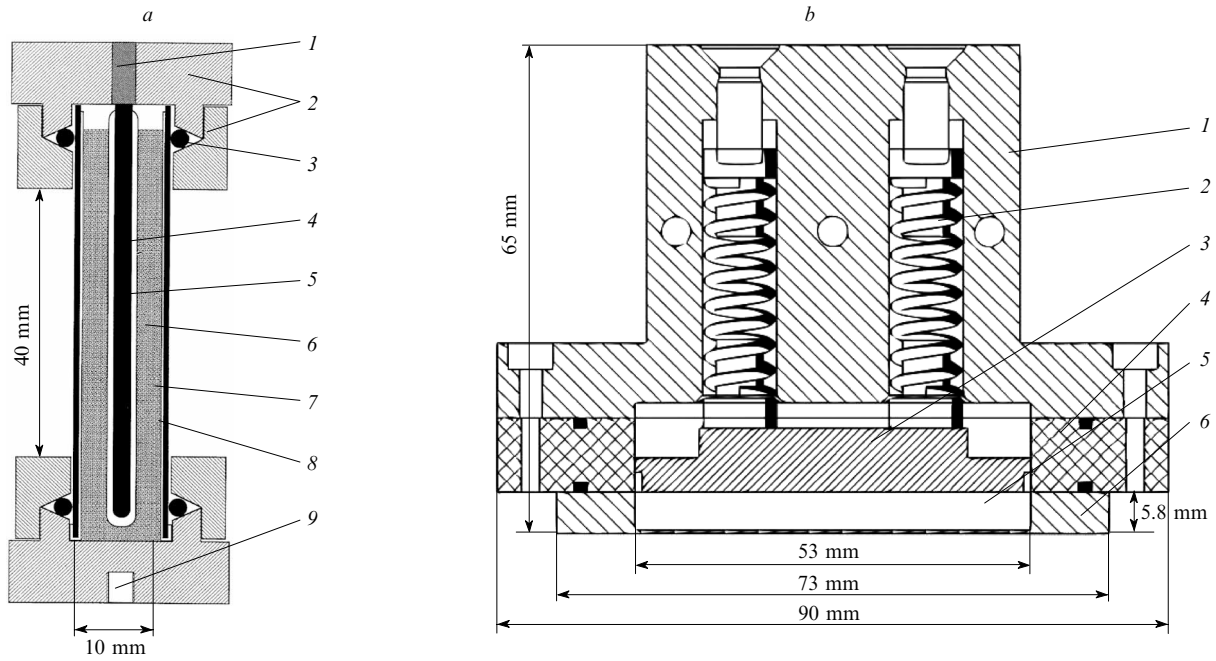


Figure 5. Designs of electrochemical cells used in the model experiments.
(*a*) The cell from Ref. 16: (*1*) seal for the Li anode, (*2*) brass collars, (*3*) an *O* ring, (*4*) Li anode, (*5*) solid polymer electrolyte and separator, (*6*) mixture of the electrode material, electrolyte and carbon black, (*7*) 100-nm layer of gold collector, (*8*) Pyrex tube, (*9*) holder;
(*b*) the cell from Ref. 18: (*1*) cell cover, (*2*) springs and valves, (*3*) copper current collector covering the Li-anode plate, (*4*) cell body, (*5*) compartment for mass of the working electrode, (*6*) aluminium current collector.

passed in the circuit. A modified version of this cell was used [17] in the *in situ* studies of the $LiMn_2O_4 \rightarrow \lambda\text{-}MnO_2$ phase transition upon electrochemical extraction of lithium from the spinel structure.

A cell for studying the processes occurring in lithium batteries using the HRPT high-resolution neutron diffractometer (PSI, Switzerland) was designed.[18] The cell design (Fig. 5 *b*) resembles an enlarged button battery. Experiments were carried out with $LiNiO_2$ and $Li_{1.1}(Ni_{1/3}Mn_{1/3}Co_{1/3})_{0.9}O_2$ (Ref. 18) as cathode materials and $Li_4Ti_5O_{12}$ (Ref. 19) as anode material. High resolution and luminosity of the diffractometer made it possible to collect high-quality neutron diffraction patterns. Changes in the lattice constants, positions of oxygen atoms and content of two lithium-containing phases, $Li_4Ti_5O_{12}$ and $Li_7Ti_5O_{12}$, in the course of charge–discharge were studied.[19] Modification of this cell allowed one to work with rather small amounts of electrode material (200–300 mg) and to observe clearly seen structural changes.[20]

Lithium intercalation into MoS_2 (a candidate for being an anode material) was studied *in situ* using an electrochemical cell with a cylindrical geometry to some extent resembling actual cylindrical lithium-ion batteries.[21] Experiments carried out at the Wombat diffractometer (ANSTO, Australia) revealed that gradual lithium insertion causes crystalline MoS_2 to undergo transformation to an intermediate crystalline phase Li_xMoS_2 (exact x value was not determined) and then to a weakly ordered semi-amorphous final phase $LiMoS_2$ characterized by a short structural coherence ($\sim$50 Å).

The results obtained in these and in many other studies showed that model experiments in electrochemical cells can provide valuable information on structural rearrangements in the active materials during the cell charge–discharge.

III.2.d. Studies on structural processes in electrode materials of actual power cells

Neutron diffraction studies of electrode materials and processes in model electrochemical cells were almost immediately followed by similar experiments with commercially available batteries having graphite anodes and cathodes made of $LiCoO_2$,[7, 10, 29, 30] $Li_xNi_yMn_zCo_{1-y-z}O_2$ [8, 31, 32] and $LiFePO_4$.[33, 34]

One of the first studies concerned charge–discharge of a commercially available battery based on $LiCoO_2$ with a nominal capacity of 2.4 A h.[7] The intensity of the neutron diffractometer enabled measurements of the neutron diffraction patterns with acceptable statistics every 15 min. As the battery was fully charged to 4.15 V, the neutron diffraction patterns were measured after each partial discharge ($\sim$18% of the total capacity) and subsequent equilibration in the open-circuit mode; this took nearly 5 h. The neutron diffraction patterns exhibited peaks from the anode, cathode, current collectors and the background from the electrolyte. They were analyzed using Rietveld method in the multiphase mode in the range of interplanar spacings from 1.30 to 1.65 Å. The authors of that study did not specify the content of lithium in the cathode material because the uncertainty related to corrections for texturing and to the limited range of interplanar spacings appeared to be too large. It was only established that discharge is accompanied by appreciable contraction of the $LiCoO_2$ structure along the c axis. In addition to the neutron diffraction peaks from the cathode material, the pattern exhibited peaks from the anode (intercalated lithium graphite of the composition

LiC_6 in the charged state of the cell). Deintercalation of the anode during battery discharge was accompanied by stepwise transitions between the LiC_6, LiC_{12} phases, *etc*, as was observed by monitoring the changes in the *d*-spacing of a strong diffraction peak from anode.

Structural transitions in electrodes of a cylindrical commercially available cell of nominal capacity of 2.6 A h were studied in more detail.[29] Neutron diffraction experiments carried out at the SPODI diffractometer (FRM II reactor) in high-resolution mode in addition to the well-studied phases LiC_6 and LiC_{12} revealed a total of seven new phases of lithium-intercalated graphite Li_xC_6 ($x = 0-0.5$) that form and vanish in the course of charge and discharge of the battery. In the neutron diffraction patterns corresponding to the $LiC_{12} \rightarrow C$ phase transition, extra diffraction peaks indicating structural modulation in the *ab* plane of the graphite lattice appeared at small angles 2θ. The superstructure was explained within the framework of the twisted bilayer model, according to which modulation appears upon twisting two neighbouring graphite layers by some angle. Based on the results obtained, a possible modulation nature of the Li_xC_6 phases at $x < 0.5$ was suggested.

Electrochemical measurements in the study of fatigue processes in a similar Li-ion battery revealed a capacity loss of 21.9% at 25 °C and 12.8% at 50 °C after 1000 charge–discharge cycles.[30] A correlation between the capacity loss and the decrease in the Li content in Li_xCoO_2 on an increase in the number of charge–discharge cycles was established upon the Rietveld refinement of the neutron diffraction patterns. The Li content decreased by ~21% (from 0.5 to 0.39 for the fully charged and from 0.94 to 0.75 the fully discharged cell) at 25 °C and by only 12% at 50 °C after 1000 charge–discharge cycles. As the number of charge–discharge cycles increased, the mass fraction of LiC_6 in the fully charged cell systematically decreased while that of LiC_{12} increased, the degradation of the anode material being more pronounced at the lower temperature.

A stepwise discharge of a cylindrical, commercially available $LiFePO_4$-based battery from the 100% state-of-charge (SOC) to the fully discharged state and *vice versa* with 30-min intervals to remove 10% SOC was studied.[33] The evolution of the intensities of the identified phases (LiC_6, LiC_{12} and LiC_{24}) during cell cycling was monitored and a previously unknown lithiated phase was discovered; the new phase exists in the range 5%–15% SOC and is assumed to be LiC_{48}. In addition, Rietveld refinement of the neutron diffraction patterns disclosed a correlation between the content of the $LiFePO_4$ and $FePO_4$ phases and the SOC. It was shown that the fully discharged cell contains ~26% of $FePO_4$ that was not converted to $LiFePO_4$.

III.3. Other features of neutron scattering

Not only neutron diffraction, but also other types of neutron scattering by matter can provide valuable information on materials and processes in power cells. For instance, information on the dynamics of light atoms in materials can be extracted from the experimentally measured incoherent inelastic scattering cross-sections. This method is particularly efficient in studies of the dynamics of hydrogen and hydrogen-containing groups because the incoherent inelastic scattering cross-section of protons is more than ten times larger than those of metal atoms and oxygen. Besides, the inelastic neutron scattering patterns, unlike optical spectra, are not influenced by any symmetry restrictions and give a full vibrational picture of compounds under study. An example of the joint neutron diffraction and inelastic neutron scattering study is provided by the simulation of the structure and vibrational spectrum of unstable nickel oxyhydroxide (β-NiOOH) that was based on the available data on the structure of and dynamics in the hydroxide β-$Ni(OH)_2$.[35]

Quasi-elastic scattering (*i.e.*, scattering involving transfer of very low energies) can be used to analyze diffusion of atoms in the liquid and solid media. This method gives information on the diffusion coefficient of ions in the battery electrolytes and on the dependence of the diffusion coefficient on temperature or on certain structure modifiers (see, *e.g.*, Ref. 36).

Small-angle neutron scattering (SANS) is used in studies of the sub-atomic structure for, *e.g.*, the determination of the geometry of large molecules in solutions, surfactant aggregates, polymers, compositional fluctuations and clustering of matter, *etc*. This is an indispensable method because it directly provides structural information on systems where the density inhomogeneities are distributed randomly or in partially ordered manner. Modern SANS facilities make it possible to cover a huge range of characteristic sizes of inhomogeneities from 10 to 10000 Å. The possibility of selective isotope substitution in particular domains of systems under study often makes SANS the only method for obtaining information on their structure on this length scale. In particular, SANS was used to study charge–discharge of a lithium battery and it was shown that the intensity of neutron scattering by the anode increases at high cycling frequency.[5] This was related to gradual cracking of graphite particles which additionally contributes to the scattering intensity.

Neutron reflectometry represents mirror reflection of neutrons from outer or inner interfaces, which is characterized by different values of the mean coherent scattering length. The phenomenon is analogous to specular reflection of light, and since the reflection index of neutrons differs only slightly from unity, total reflection is only possible at small angles (usually, the critical angle is of the order of a few angular minutes). At present, this method is of limited use in the studies of batteries, but some examples of its application are now available. The technique is sensitive to changes in the scattering density in the direction that is perpendicular to the interface. Also, it enables rather accurate determination of layer thicknesses. The possibility of *in situ* scanning an interface representing a layer of solid electrolyte to a depth of 10 nm with a resolution of about 1 nm was reported.[37]

Modern neutron reflectometers enable the use of polarized primary neutron beam to separate the magnetic contribution to the reflection coefficient. Besides specular reflection, one can detect diffuse scattering (it appears owing to imperfection of the reflecting layer) and analyze corresponding data in order to estimate the surface roughness or find discontinuity regions on the surface.

Thermal neutrons may be used in introscopy of real devices (radiography and imaging experiments). For instance, preliminary experimental studies of hydrogen migration in the course of discharge of an alkaline AA battery were carried out at the specialized Neutron Imaging Facility (NIF) at NIST (USA).[38] The neutron tomogram slice through the cell (Fig. 6) demonstrates the clearly resolved anode (at the centre), the separator (circle in the

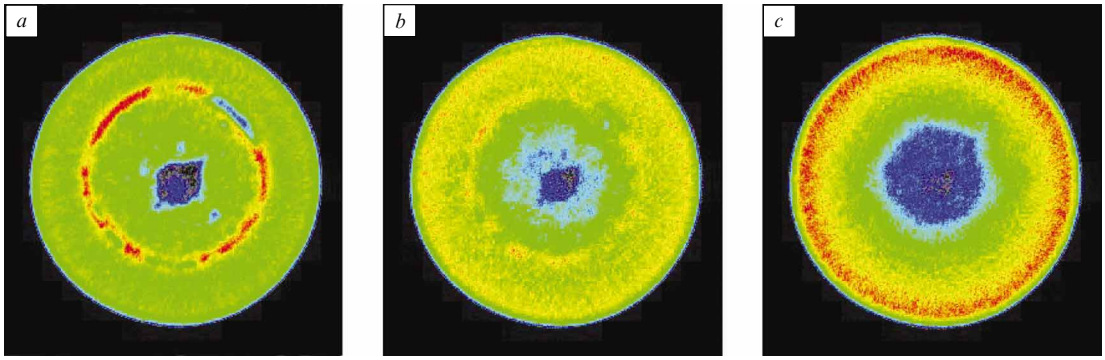


Figure 6. Neutron tomogram slices through the alkaline AA cell during its discharge.[38]
Different grey tones denote different degrees of neutron absorption by the material, which can be related to the hydrogen content in the material; (*a*) initial (charged) state; (*b*) the state after 17.5-h discharge at a d.c. of 50 mA; (*c*) the state after 52.5-h discharge at a d.c. of 50 mA. Changes in neutron absorption allow one to monitor migration of hydrogen ions.

middle part of the tomogram) and the cathode (at the periphery). Different colours denote different degrees of neutron absorption by the structural materials of the cell. Changes in the colours are related to migration of hydrogen ions in the course of cell discharge, so one can estimate the content of hydrogen and obtain information on the kinetics of the process, the homogeneity of materials with respect to hydrogenation/dehydrogenation, *etc*. The results obtained in a continuation of these studies were reported in more detail elsewhere;[39,40] in particular, it was shown how neutron radiography can be used to observe swelling of electrodes during the cell charge.

The potential and limitations of neutron introscopy of lithium-ion batteries were reviewed.[41]

IV. Neutron scattering experiments at the IBR-2 reactor: a survey

The IBR-2 high-flux pulsed research reactor † operates at the Frank Laboratory of Neutron Physics (Joint Institute for Nuclear Research, Dubna, Russian Federation) since 1984. The modern complex of spectrometers of the IBR-2 pulsed reactor (Fig. 7) includes seven diffractometers (HRFD, DN-2, DN-6, SKAT, EPSILON, FSD, DN-12), a SANS spectrometer (YuMO), three reflectometers

† Information on the IBR-2 reactor can be found in Ref. 42 and is available at URL http://flnp.jinr.ru/. Information concerning submission of applications for beam time at the IBR-2 reactor is also available at the website specified.

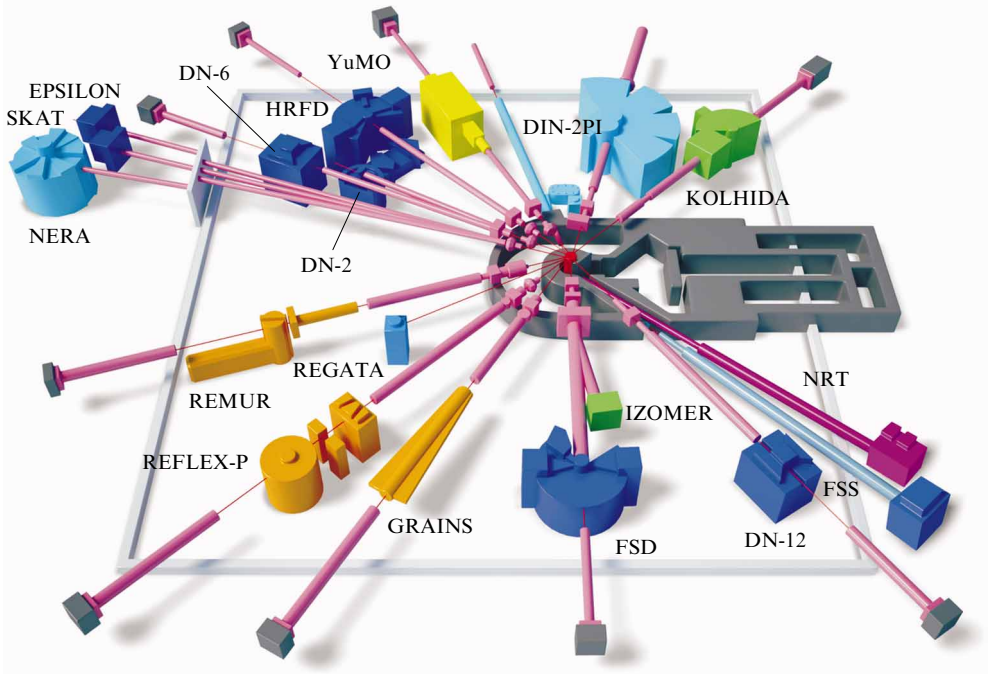


Figure 7. A schematic of the experimental halls of the IBR-2 reactor.
The reactor is at the centre. Neutron beams are provided to spectrometers through channels in the biological shielding *via* beam tubes. The GRAINS, DN-6, NRT and FSS spectrometers are under construction.

(REMUR, REFLEX-P, GRAINS), two inelastic neutron scattering spectrometers (NERA, DIN-2PI), two nuclear physics facilities (IZOMER and KOLHIDA) and an irradiation facility for neutron activation analysis (REGATA). A spectrometer for neutron radiography and tomography (NRT) is under construction; installation of the FSS diffractometer delivered from GKSS (Geesthacht, Germany) is planned. All spectrometers utilize the time-of-flight technique. A feature of the upgraded reactor is the record-high pulsed neutron flux (up to 10^{16} neutron cm^{-2} s^{-1}) and upcoming commissioning of a number of cold moderators.

An RTD diffractometer for real-time neutron experiments is also under construction; it will replace DN-2. The RTD diffractometer will be equipped with a multidetector system for detection of scattered neutrons, namely, small-angle scattering detectors (for SANS), near-90° angle detectors (medium and large d_{hkl} values), and back-scattering detectors (medium and small d_{hkl} values). This will cover the range of interplanar spacings from 1 to 30 Å with a resolution of the order of 1%–5%. Also, design of the equipment for specifying and maintaining necessary conditions in real-time experiments (including a model electrochemical cell adapted to geometry of RTD).

IV.1. Structural experiments at the IBR-2 reactor

Most structural experiments at the IBR-2 reactor are carried out using the high-resolution Fourier-diffractometer (HRFD)[43] with the Fourier correlation technique. The instrument has two modes for measuring the diffraction patterns, *viz*., high-resolution with respect to interplanar spacing (using a Fourier chopper and correlation electronics, $\Delta d/d \approx 0.001$) and high-intensity mode (conventional TOF method, $\Delta d/d \approx 0.01$). In addition to the determination or refinement of the atomic and magnetic structures, the HRFD is suitable for analyzing the sample microstructure, *i.e*., for determining the characteristic sizes of coherently scattering blocks and detecting microstrains in crystallites. The width of a diffraction peak is influenced by the finite block size and microstrain, the contributions of these factors to the peak width depend on d_{hkl} in different manner, which allows them to be separated. The resolution of the HRFD in the TOF mode can be described by a simple analytical expression. The experimentally measured diffraction peak width (W_{hkl}) depends on d_{hkl} as follows:

$$W^2 = C_1 + (C_2 + C_3)\,d^2 + C_4\,d^4$$

where the constants C_1 and C_2 are determined by the resolution function of the diffractometer, $C_3 \approx (2\,\varepsilon)^2$, $C_4 \approx (1/L)^2$, ε is the microstrain and L is the characteristic size of coherently scattering blocks. Having known the resolution function and having plotted the $W^2(d^2)$ dependences for a sufficiently wide range of interplanar spacings, one can determine ε and L.

One of the first examples of structure determination using the HRFD is a study of ternary hydride Li_2BeD_4 comprising atoms of three light elements.[44] The structure solved *ab initio* by joint analysis of the X-ray and neutron diffraction patterns appeared to be monoclinic (space group $P2_1/c$, $V_c \approx 500$ Å^3) and included almost regular BeD_4 tetrahedra (Li–D distance varied in the range of 1.40–1.44 Å) and Li atoms that are located in the structure interstices (Fig. 8). The bond lengths in the LiD_n polyhedra (octahedra and tetrahedra) varied from 1.88 to 2.18 Å.

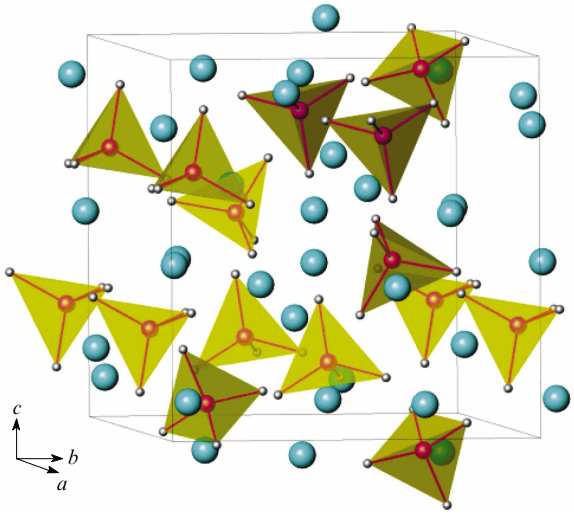


Figure 8. Crystal structure Li_2BeD_4.[44]
Beryllium atoms are within the BeD_4 tetrahedra; individual solid circles denote Li^+ ions.

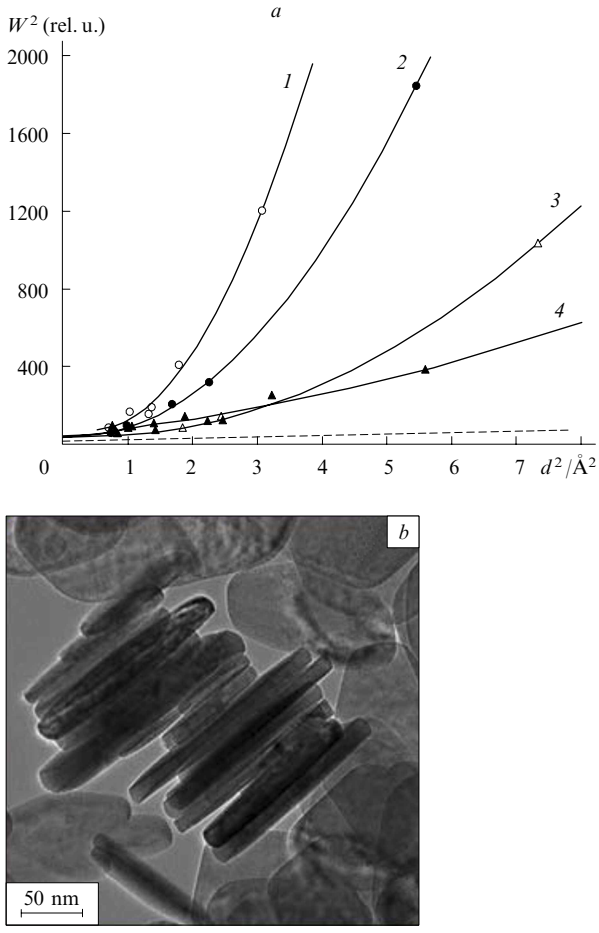


Figure 9. The width of neutron diffraction peaks of β-$Ni(OH)_2$ for different values of the index l (*1*–*3*) and $Mg(OH)_2$ (for all *hkl*) (*4*) plotted *vs*. interplanar spacing (*a*)[35] and an electron micrograph of β-$Ni(OH)_2$ particles (*b*).[45]
(*1*) $l > 1$, (*2*) $l = 1$, (*3*) $l = 0$; solid lines correspond to approximation of experimental points by a 4th order polynomial, dashed line is the resolution function for the diffractometer.

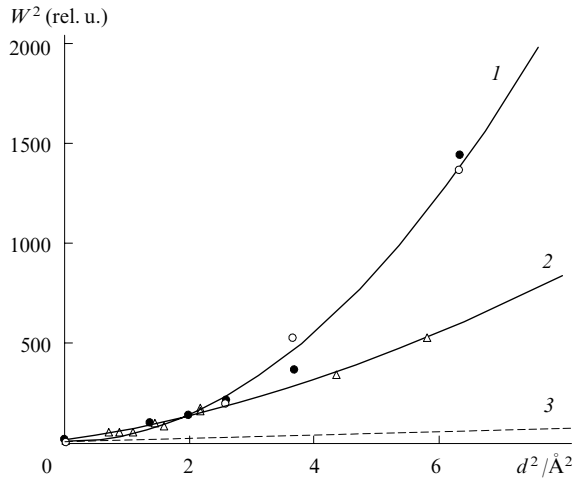


Figure 10. The width of magnetic (*1*) and crystalline (*2*) diffraction peaks of NiO (crystallite size $L \approx 100$ nm) plotted *vs.* interplanar spacing and the resolution function of the diffractometer (*3*) measured using a reference sample.
Nonlinear character of the curves passing through the experimental points indicates a finite size of the crystalline and magnetic domains.

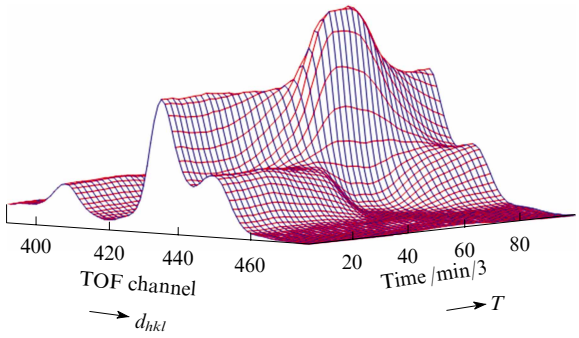


Figure 11. Characteristic region of the neutron diffraction patterns (data acquisition every 80 s) of substituted copper ferrite $CuLi_{0.1}V_{0.1}Fe_{1.8}O_4$ continuously heated from 400 to 800 K and subsequently cooled to 400 K.[48]
TOF channel: the range from 400 to 460 corresponds to the range of interplanar spacings d_{hkl} from 2.3 to 2.7 Å. At zero time (see the time/temperature scale), the sample is at 400 K, being heated to 800 K (mid-point of the time/temperature scale) at a rate of ~ 5 K min^{-1} and then cooled to 400 K (end point of the time/temperature scale) at the same rate. The shape of the diffraction peaks changes owing to transition from the tetragonal to cubic phase (at 740 K) and *vice versa*.

The morphology of β-$Ni(OH)_2$ particles was determined (see above).[35] This compound is used as a cathode in Ni–Cd batteries. Experimental values of the diffraction peak widths for β-$Ni(OH)_2$ and β-$Mg(OH)_2$ are plotted *vs.* interplanar spacing in Fig. 9 *a*. Based on the dependence of the anisotropy of the diffraction peak on the Miller indices, it was established that β-$Ni(OH)_2$ particles are disk-shaped and their characteristic sizes are about 350 Å (diameter) and nearly 150 Å (thickness). These results were obtained owing to high resolution of the HRFD; they agree with the electron microscopy data (Fig. 9 *b*).[45] As can be seen, the particles have the shape of disks ~ 1500 Å in diameter and ~ 200 Å thick. Discrepancies between the estimates can be due to amorphous structure of the exterior of disks, which does not contribute to diffraction.

A similar problem was solved in a study[46] of changes in the atomic and magnetic structures of NiO nanopowders from the standpoint for formation of coherently scattering domains. It was found that the 'diffraction' sizes of the crystalline and magnetic domains (*i.e.*, domains with long-range order) were almost the same as the crystallite size decreased down to nearly 140 nm. However, as the crystallite size further decreased to ~ 100 nm, the difference between the 'diffraction' sizes abruptly increased by a factor of 2.5 (Fig. 10), namely, the 'diffraction' size of crystalline domains agrees with the expected value $L = 98 \pm 4$ nm, whereas the size of ordered magnetic domains is about 40 nm. Probably, crystallites comprise 'cores' with long-range magnetic ordering and magnetically disordered peripheral regions.

IV.2. Real-time neutron diffraction experiments

In situ real-time neutron diffraction experiments at the IBR-2 reactor (investigations of transient processes in crystalline materials) can be carried out using the HRFD and DN-2 facilities. The high luminosity of the DN-2 allowed the diffraction patterns to be measured within 1 min.[47] Usually, the instrument operated in the parametric mode, *i.e.*, a certain external parameter (temperature, humidity, electric potential, *etc.*) was gradually varied in a specified range.

In situ experiments[48] using DN-2 gave detailed information on the structural phase transition in substituted copper ferrite $CuLi_{0.1}V_{0.1}Fe_{1.8}O_4$ having interesting magnetic and dielectric properties. Heating at 740 K is accompanied by a reversible structural transition from the tetragonal phase (space group $I4_1/amd$) to the more symmetric cubic phase (space group $Fd3m$) with a hysteresis of about 50 K. Changes in the neutron diffraction patterns in the characteristic range of interplanar spacings on continuous heating from 400 to 800 K and subsequent cooling to 400 K are shown in Fig. 11. In addition to the natural changes in the lattice constants and atomic coordinates of oxygen, this experiment revealed the appearance of strong anisotropic microstrain at interfaces upon the transition.

IV.3. Experiments with lithium-ion batteries

Systematic studies of power cells using spectrometers at the IBR-2 reactor have been started only recently and are restricted to the diffraction experiments. Interesting results were obtained in a study[49] of two flat batteries (Fig. 12) with a pristine $LiFePO_4$ cathode (battery No. 1, capacity ~ 2 A h) and with a vanadium-doped lithium ferrous phosphate $LiFePO_4:V_\delta$, $\delta \approx 0.01$ (battery No. 2, capacity ~ 10 A h). Both batteries had a graphite anode.

The batteries were charged and discharged using a galvanostat at a rate of $C/10$ (*i.e.*, battery No. 1 and No. 2 were charged at a d.c. of 200 mA and 1 A, respectively) at voltages between 2.5 and 3.8 V. The neutron diffraction data were collected *in situ* using the HRFD (high-intensity, medium resolution) with a 10-min acquisition time per diffraction pattern in real time. High resolution was used to obtain information on the phase composition and on the



Figure 12. Photograph of the Li-ion battery of capacity 10 A h (at the centre) during the neutron diffraction experiment. Fragments of collimator that forms the incident neutron beam (on the right).

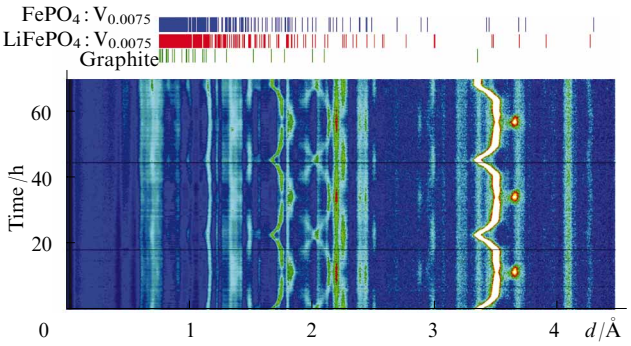


Figure 13. Evolution of the neutron diffraction patterns from battery No 2, measured during three charge–discharge cycles at a rate of $C/10$.[49]

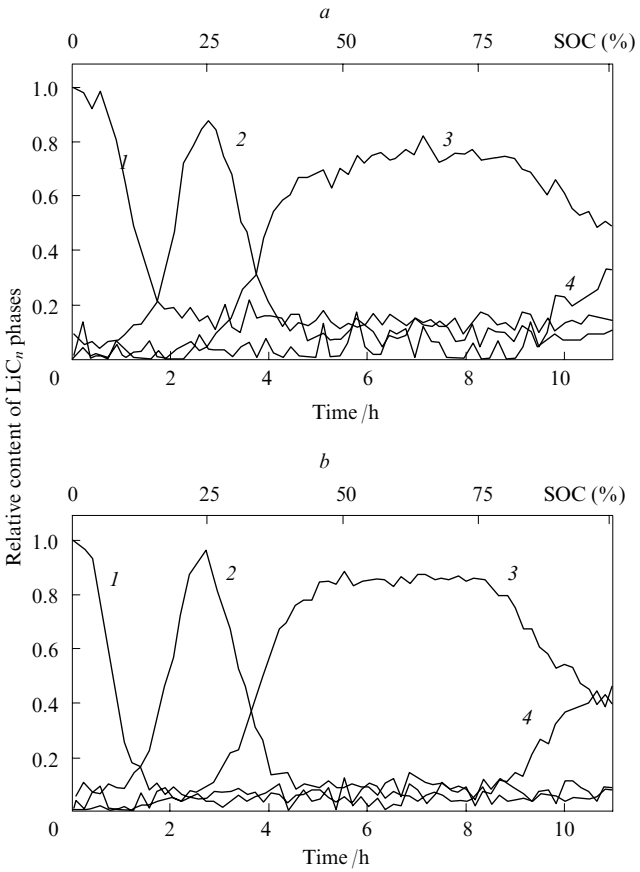


Figure 14. The content of LiC_n phases in batteries No 1 (*a*) and No 2 (*b*) plotted *vs.* time or SOC during one charge cycle. Extracted from the relative changes in the intensities of corresponding neutron diffraction peaks.[49]
Phase: C (*1*), LiC_{27} (*2*), LiC_{18}, LiC_{12} (*3*) and LiC_6 (*4*).

structure of the anode and cathode materials in the steady state at a particular SOC of the battery. For instance, at 50% SOC the diffraction pattern exhibited peaks corresponding to six structural phases.

The evolution of the 2D diffraction patterns obtained *in situ* during three charge–discharge cycles (cycle duration was ~20 h) is shown in Fig. 13. Positions of the diffraction peaks of the three main structural phases in the initial state are denoted by vertical lines at the top. The most intense lines in the range from 3.2 to 3.7 Å ('anode window') are attributed to the graphite electrode. A number of intense peaks in the range 2.2–3.2 Å ('cathode window') correspond to the $LiFePO_4$ and $FePO_4$ phases.

This type of experiments is, in particular, aimed at determining the relative content of the cathode phases, $LiFePO_4$ and $FePO_4$, as function of the battery charge. A Rietveld refinement of the neutron diffraction patterns allows the relative content to be determined with an accuracy of ~5%.

It was shown that from the standpoint of delithiation vanadium-doped lithium iron phosphate is more efficient than pristine lithium iron phosphate. Also, it was found that a considerable proportion of the cathode material is not involved in the battery operation.

An analysis of the diffraction peaks of the anode window made it possible to trace successive formation of several LiC_n phases upon lithium insertion into graphite (Fig. 14). Initially, the interplanar spacing between graphite layers gradually increases, *i.e.*, lithium is inserted between the layers. Next, the interplanar spacing increases only slightly, which corresponds to lithium insertion into the basal plane of the graphite structure. The formation of the final phase, LiC_6, during the charge of the battery is clearly detected from the a step-like appearance of the diffraction peak at $d \approx 3.67$ Å. In the fully charged battery, the LiC_6 phase occupies ~50% of the initial volume of the graphite electrode, the remaining volume being filled with phases with lower lithium content (mainly LiC_{12}). In battery No. 2 the content of the LiC_6 phase in the anode material is ~10% higher than in battery No. 1.

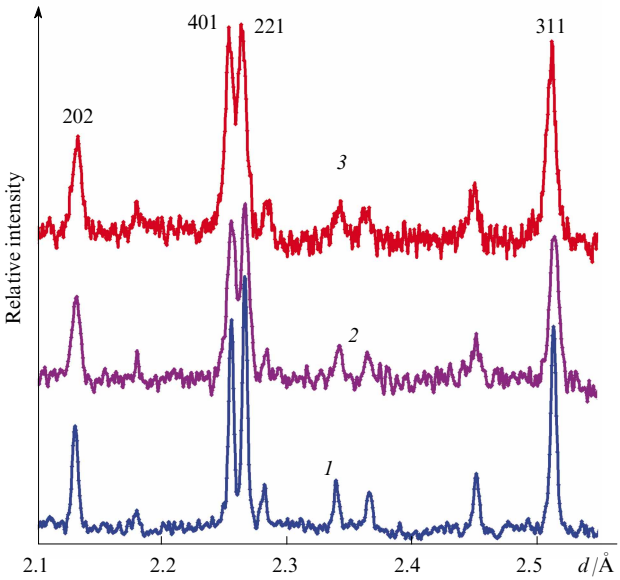


Figure 15. Characteristic regions of the neutron diffraction patterns of $LiFePO_4:V_\delta$ with different vanadium content measured in the high-resolution mode.[49]
δ (%): 0 (*1*), 0.75 (*2*) and 5 (*3*). The peak width and the incoherent background increase with increasing vanadium content. Shown are the Miller indices of the most intense peaks.

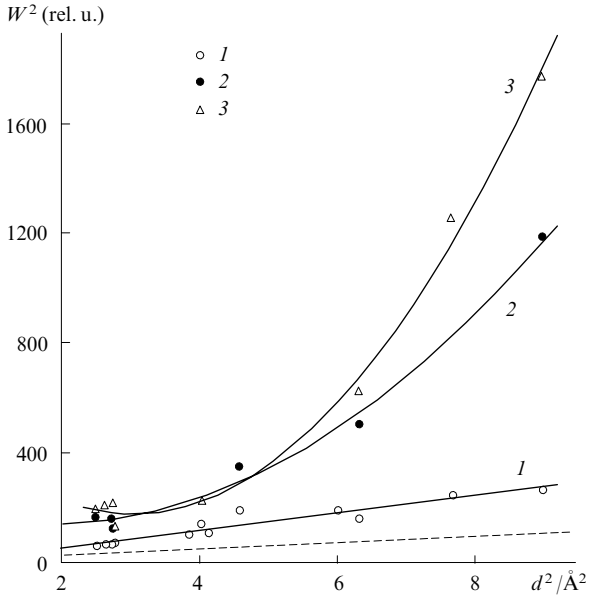


Figure 17. The widths of neutron diffraction peaks plotted *vs.* interplanar spacing.[49]
δ (%): 0 (*1*), 0.75 (*2*) and 5 (*3*). The peak widths of pristine $LiFePO_4$ fall on the straight line (*1*), whereas the peak widths of vanadium-doped $LiFePO_4$ fall on parabolas (*2*, *3*) owing to small size of coherent scattering domans. The dashed line is the resolution function of the diffractometer measured using a reference sample.

To refine the structural parameters of the cathode materials, the neutron diffraction patterns from powdered $LiFePO_4$ and $LiFePO_4:V_\delta$ ($\delta = 0$, 0.75%, 2% and 5%) samples were collected using the HRFD at several temperatures (Fig. 15 presents the room-temperature neutron diffraction patterns). The atomic structures of all samples were in good agreement with published data,[12] the atomic coordinates almost coincided at all δ values. Attempts to determine which cations are replaced by vanadium on doping of $LiFePO_4$ led to ambiguous results; structure refinement for $LiFePO_4:V_\delta$ with $\delta = 2\%$ and 5% indicated that a number of lithium and iron sites are vacant. However, this result seems not to be reliable because of strong correlations between the atomic occupancies and thermal factors. The lattice constants, which are most accurately determined from the neutron diffraction data, demonstrate noticeable variations upon doping with vanadium (Fig. 16); this seems to be an indication of vanadium insertion into the structure.

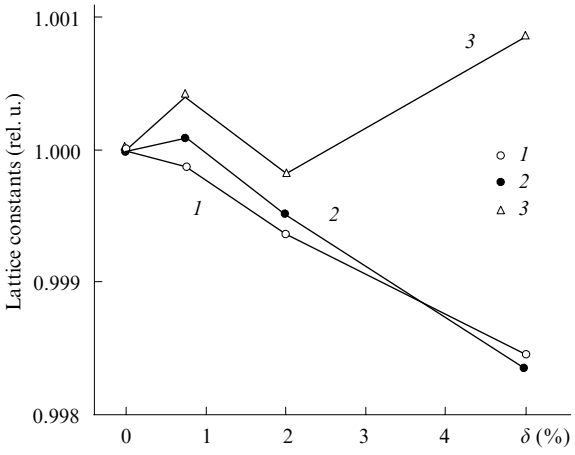


Figure 16. Relative changes in the constants *a* (*1*), *b* (*2*) and *c* (*3*) of $LiFePO_4:V_\delta$ rhombohedral cell with increasing vanadium content.[49]
Experimental points: obtained from results of measurements using HRFD.

The $LiFePO_4:V_\delta$ samples with $\delta = 0.75\%$ and especially $\delta = 5\%$ exhibit significant changes in the microstructural parameters compared to those of pristine $LiFePO_4$, which manifest themselves in broadening of the diffraction peaks with increasing δ. An analysis showed that the broadening is due to the size effect (Fig. 17), *i.e.*, vanadium insertion into $LiFePO_4$ causes a considerable decrease in the characteristic size of the coherently scattering domains from a few thousands of Å to nearly ~400 Å. This can be interpreted as significant increase in the defectiveness of the structure, which correlates with the better electrochemical properties of vanadium-doped lithium iron phosphate compared to pristine lithium iron phosphate.

Summing up, neutron diffraction experiments with batteries No. 1 and No. 2 carried out using the HRFD neutron diffractometer at the IBR-2 pulsed reactor enabled real-time monitoring of electrode processes in the course of charge–discharge cycling. The results obtained enable reliable identification of the appearing structural phases and quantitative analysis of the kinetics of phase transformations in the anode and cathode materials. An important feature of these experiments consists in the possibility to switch

between two different operational modes of the diffractometer, namely, high-intensity and high-resolution ones, without changing the scattering geometry. Clearly, TOF-neutron diffraction at the HRFD is a very promising method of investigation of materials constituting lithium-ion batteries and transient processes in them.

V. Conclusion

The available experience in application of the X-ray and neutron scattering to electrochemical studies shows that it is these methods that play an important role in obtaining information needed for understanding the mechanisms of processes occurring in rechargeable energy sources and, therefore, for improvement of their operating properties.

A strategy of scientific research on novel materials for power cells is as follows. Initial tests of a material from the electrochemical point of view are followed by detailed studies of its atomic structure using X-ray and neutron scattering. Neutron experiments provide a better insight into the structural features of the material and make it possible to refine the cation distribution, to analyze the behaviour of the material in a wide temperature range and to determine the magnetic properties. Usually, the best results are obtained in joint X-ray (or synchrotron radiation) and neutron diffraction studies. Undoubtedly, structural studies of electrochemical materials using neutron diffraction and, in a broader sense, neutron scattering will be performed with increasing intensity.

Prospects for these investigations at the IBR-2 reactor seem to be quite obvious. The level of research activity using the available spectrometers is comparable with international standards. New fields of application will open upon installation of a facility for neutron introscopic experiments. This facility will not only operate in the currently-'cutting-edge' modes (see, *e.g.*, Ref. 50), but will also provide an extra option, *viz.*, higher contrast in the detection of transmitted neutron beams at different wavelengths ranges.

This review has been written with the financial support from the Russian Science Foundation (Project No. 14-12-00896).

References

1. K Mizushima, P C Jones, P J Wiseman, J B Goodenough *Mater. Res. Bull.* **15** 783 (1980)
2. A K Padhi, K S Nanjundaswamy, J B Goodenough *J. Electrochem. Soc.* **144** 1188 (1997)
3. J B Goodenough, Y Kim *Chem. Mater.* **22** 587 (2010)
4. C Masquelier, L Croguennec *Chem. Rev.* **113** 6552 (2013)
5. H Wang, R G Downing, J A Dura, D S Hussey, in *Polymers for Energy Storage and Delivery: Polyelectrolytes for Batteries and Fuel Cells (ACS Symp. Ser.* Vol. 1096) (Eds K Page, C Soles, J Runt) (New York: American Chemical Society, 2012) p. 91
6. N Sharma, V K Peterson *J. Solid State Electrochem.* **16** 1849 (2012)
7. M A Rodriguez, D Ingersoll, S C Vogel, D J Williams *Electrochem. Solid-State Lett.* **7** A8 (2004)
8. H Liu, C R Fell, K An, L Cai, Y S Meng *J. Power Sources* **240** 772 (2013)
9. P S Whitfield, I J Davidson, P W Stephens, L M D Cranswick, I P Swainson *Z. Kristallogr. (Suppl.)* **26** 483 (2007)
10. N Sharma, V K Peterson, M M Elcombe, M Avdeev, A J Studer, N Blagojevic, R Yusoff, N Kamarulzaman *J. Power Sources* **195** 8258 (2010)
11. J Li, J Zhang, X Zhang, C Yang, N Xu, B Xia *Electrochim. Acta* **55** 927 (2010)
12. G Rousse, J Rodriguez-Carvajal, S Patoux, C Masquelier *Chem. Mater.* **15** 4082 (2003)
13. P S Whitfield, I J Davidson, L M D Cranswick, I P Swainson, P W Stephens, in *Advances in X-ray Analysis. Proceedings of the Denver X-ray Conference,. Colorado Springs, USA, 2005* Vol. 49, p. 149
14. M Yashima *J. Ceram. Soc. Jpn.* **117** 1055 (2009)
15. S-I Nishimura, G Kobayashi, K Ohoyama, R Kanno, M Yashima, A Yamada *Nat. Mater.* **7** 707 (2008)
16. Õ Bergstöm, A M Andersson, K Edström, T Gustafsson *J. Appl. Cryst.* **31** 823 (1998)
17. H Berg, H Rundlöv, J O Thomas *Solid State Ionics* **144** 65 (2001)
18. F Rosciano, M Holzapfel, W Scheifele, P Novvk *J. Appl. Cryst.* **41** 690 (2008)
19. J-F Colin, V Godbole, P Novák *Electrochem. Commun.* **12** 804 (2010)
20. V A Godbole, M Hess, C Villevieille, H Kaiser, J-F Colin, P Novák *RSC Adv.* **3** 757 (2013)
21. N Sharma, G Du, A J Studer, Z Guo, V K Peterson *Solid State Ionics* **199–200** 37 (2011)
22. F Barde, M R Palacin, Y Chabre, O Isnard, J-M Tarascon *Chem. Mater.* **16** 3936 (2004)
23. J J Biendicho, M Roberts, C Offer, D Noréus, E Widenkvist, R I Smith, G Svensson, K Edström, S T Norberg, S G Eriksson, S Hull *J. Power Sources* **248** 900 (2014)
24. G Du, N Sharma, V K Peterson, J A Kimpton, D Jia, Z Guo *Adv. Funct. Mater.* **21** 3990 (2011)
25. N Sharma, M V Reddy, G Du, S Adams, B V R Chowdari, Z Guo, V K Peterson *J. Phys. Chem. C* **115** 21473 (2011)
26. N Sharma, X Guo, G Du, Z Guo, J Wang, Z Wang, V K Peterson *J. Am. Chem. Soc.* **134** 7867 (2012)
27. J Bianchini, B Leriche, J-L Laborier, L Gendrin, E Suard, L Croguennec, C Masquelier *J. Am. Chem. Soc.* **160** A2176 (2013)
28. W K Pang, N Sharma, V K Peterson, J-J Shiu, S-H Wu *J. Power Sources* **246** 464 (2014)
29. A Senyshyn, O Dolotko, M J Mühlbauer, K Nikolowski, H Fuess, H Ehrenberg *J. Electrochem. Soc.* **160** A3198 (2013)
30. O Dolotko, A Senyshyn, M J Mühlbauer, K Nikolowski, F Scheiba, H Ehrenberg *J. Electrochem. Soc.* **159** A2082 (2012)
31. X -L Wang, K An, L Cai, Z Feng, S E Nagler, C Daniel, K J Rhodes, A D Stoica, H D Skorpenske, C Liang, W Zhang, J Kim, Y Qi, S J Harris *Sci. Rep.* **2** 747 (2012)
32. O Dolotko, A Senyshyn, M Mühlbauer, K Nikolowski, H Ehrenberg *J. Power Sources* **255** 197 (2014)
33. M A Rodriguez, M H van Benthem, D Ingersoll, S C Vogel, H M Reiche *Powder Diffr.* **25** 143 (2010)
34. C-W Hu, N Sharma, C-Y Chiang, H-C Su, V K Peterson, H-W Hsieh, Y-F Lin, W-C Chou, B-Y Shew, C-H Lee *J. Power Sources* **244** 158 (2013)
35. V Yu Kazimirov, M B Smirnov, L Bourgeois, L Guerlou-Demourgues, L Servant, A M Balagurov, I Natkaniec, N R Khasanova, E V Antipov *Solid State Ionics* **181** 1764 (2010)
36. S K Fullerton-Shirey, J K Maranas *Macromolecules* **42** 2142 (2009)
37. J E Owejan, J P Owejan, S C DeCaluwe, J A Dura *Chem. Mater.* **24** 2133 (2012)
38. D Hussey, in *216th ECS Meeting Abstracts, Vienna, 2009* Abstr. 234
39. G V Riley, D S Hussey, D L Jacobson *ECS Transact.* **25** 75 (2010)

40. J B Siegel, X Lin, A G Stefanopoulou, D S Hussey, D L Jacobson, D Gorsich *J. Electrochem. Soc.* **158** A523 (2011)
41. L G Butler, E H Lehmann, B Schillinger *Phys. Proc.* **43** 331 (2013)
42. V L Aksenov *Crystallogr. Rep.* **52** 372 (2007) [*Kristallografiya* **52** 396 (2007)]
43. A M Balagurov *Neutron News* **16** 8 (2005)
44. B M Bulychev, R V Shpanchenko, E V Antipov, D V Sheptyakov, S N Bushmeleva, A M Balagurov *Inorg. Chem.* **43** 6371 (2004)
45. D Chen, L Gao *Chem. Phys. Lett.* **405** 159 (2005)
46. A M Balagurov, I A Bobrikov, J Grabis, D Jakovlevs, A Kuzmin, M Maiorov, N Mironova-Ulmane *IOP Conf. Ser.: Mater. Sci. Eng.* **49** 012021 (2013)
47. A M Balagurov, G M Mironova *Mater. Sci. Forum* **133 – 136** 397 (1993)
48. A M Balagurov, E P Kozlova, G M Mironova, I Jacyna-Onyszkiewicz *Phys. Status Solidi A* **136** 57 (1993)
49. I A Bobrikov, A M Balagurov, C-W Hu, C-H Lee, T-Y Chen, S Deleg, D A Balagurov *J. Power Sources* **258** 356 (2014)
50. E H Lehmann, P Vontobel, G Frei, G Kuehne, A Kaestner *Nucl. Instrum. Methods Phys. Res., Sect. A* **651** 1 (2011)